Available online at www.sciencedirect.com
SCIENCE DIRECT®
Applied Geochemistry 20 (2005) 2038–2048
Applied Geochemistry
www.elsevier.com/locate/apgeochem

Ferric iron in sediments as a novel CO_2 mineral trap: CO_2–SO_2 reaction with hematite

James L. Palandri *, Robert J. Rosenbauer, Yousif K. Kharaka

US Geological Survey, 345 Middlefield Road, Menlo Park, CA 94025, USA

Received 17 August 2004; accepted 14 June 2005
Editorial handling by I. Hutcheon

Abstract

Thermodynamic simulations of reactions among SO_2-bearing CO_2-dominated gas, water and mineral phases predict that Fe^{III} in sediments should be converted almost entirely to dissolved Fe^{II} and siderite ($FeCO_3$), and that SO_2 should simultaneously be oxidized to dissolved sulfate. The reactions are however, subject to kinetic constraints which may result in deviation from equilibrium and the precipitation of other metastable mineral phases. To test the prediction, a laboratory experiment was carried out in a well stirred hydrothermal reactor at 150 °C and 300 bar with hematite, 1.0 m NaCl, 0.5 m NaOH, SO_2 in quantity sufficient to reduce much of the iron, and excess CO_2. The experiment produced stable siderite and metastable pyrite and elemental S. Changes in total dissolved Fe are consistent with nucleation of pyrite at ~17 h, and nucleation of siderite at ~600 h. Dissolution features present on elemental S at the conclusion of the experiment suggest nucleation early in the experiment. The experiment did not reach equilibrium after ~1400 h, as indicated by coexistence of hematite with metastable pyrite and elemental sulfur. However, the results confirm that Fe^{III} can be used to trap CO_2 in siderite if partly oxidized S, as SO_2, is present to reduce the Fe with CO_2 in the gas phase.

1. Introduction

Combustion of fossil fuels and other human activities have contributed to a 30% increase in atmospheric CO_2 since 1850 (Bruant et al., 2002; Falkowski et al., 2000). This greenhouse gas is a likely significant contributor to global climate change. Within the last decade, considerable research has been conducted into reducing CO_2 emissions to the atmosphere, including the capture of CO_2 from power plant flue gas, and storage or sequestration of in geologic formations, terrestrial biomass, or the oceans (e.g., Bergman and Winter, 1995; Gunter et al., 1997, 2000; Harrison and Wendlandt, 1995; Hitchon, 1996; Kaszuba et al., 2003; McPherson and Cole, 2000; Spycher et al., 2003; White et al., 2003; Wolf et al., 2004). Sedimentary formations offer an enormous potential repository for CO_2 sequestration, where CO_2 may be injected and stored as a supercritical fluid, as a dissolved component in formation water, or trapped in minerals. Studies of in situ mineral trapping of CO_2 (Gunter et al., 2000, 1997; Johnson et al., 2001; Kaszuba et al., 2003; Pruess et al., 2001) generally consider the use of Ca-bearing arkosic, Mg-bearing illitic, or Fe^{II}-bearing glauconitic sediments to trap CO_2 in calcite, magnesite, siderite, or ankerite ($CaFe(CO_3)_2$). Glauconitic beds, which contain Fe^{II} that could precipitate in siderite or

* Corresponding author. Present address: Department of Geological Sciences, 1272 University of Oregon, Eugene, OR 97403, USA. Tel.: +1 541 346 5990; fax: +1 541 346 4692.
E-mail address: palandri@efn.org (J.L. Palandri).

0883-2927/$ - see front matter © 2005 Elsevier Ltd. All rights reserved.
doi:10.1016/j.apgeochem.2005.06.005

ankerite, are generally of limited thickness and geographical occurrence.

In contrast to glauconitic sediments, Fe^{III}-bearing sediments, including redbeds, are of widespread geographic distribution and generally great thickness. In addition they commonly have high porosity and permeability. As such, they have great potential to trap CO_2 in siderite and/or ankerite, if the Fe^{III} can be reduced to Fe^{II}. The authors propose the use of SO_2 gas as an Fe reductant. Sulfur dioxide gas is a logical choice, because it is already a component of the CO_2-bearing flue gas produced by combustion of S-bearing fossil fuel.

Herein the authors examine the possibility of using SO_2 to reduce Fe^{III} to Fe^{II}, thereby allowing Fe to precipitate with CO_2 as siderite. Using hematite as a proxy for Fe^{III} in sediments, the authors first determined using theoretical calculations if the products of the reaction:

$$Fe_2O_3\ (\text{rock}) + 2CO_2 + SO_2 + H_2O = 2FeCO_3\ (\text{siderite}) + H_2SO_4 \quad (1)$$

are favored by equilibrium thermodynamics. A laboratory experiment was then performed to determine if the relative reaction kinetics favored the desired siderite product, rather than other metastable phases.

2. Details of the problem

Previous investigations have shown that: (1) dissolved sulfide reacts with Fe^{III} in sediments to produce solid iron sulfide and dissolved sulfate, and (2) SO_2 reacts with liquid water to produce dissolved sulfide. Experimental and theoretical studies of disposal in redbeds of H_2S extracted from sour natural gas have shown that dissolved sulfide apparently reacts quickly with Fe^{III} in minerals to produce amorphous iron sulfide (FeS-am), dissolved sulfate, and metastable thiosulfate (Palandri, 2000):

$$4Fe_2O_3\ (\text{rock}) + 9H_2S\ (\text{aq}) = 8FeS(\text{amorphous}) + H_2SO_4\ (\text{aq}) + 8H_2O \quad (2)$$

Given that Fe^{III} reduction is accompanied by S oxidation, the reduced Fe^{II} must subsequently react with additional reduced S (HS^-, H_2S) to produce FeS-am. This suggests at least a two step reaction mechanism, and that all of the Fe eventually residing in sulfide minerals likely previously existed as dissolved Fe^{II}-bearing species.

Field observations of volcanic systems and thermodynamic modeling (Getahun et al., 1996; Symonds et al., 2001) show that SO_2 gas reacts quickly to produce H_2S and H_2SO_4 in an aqueous disproportionation reaction:

$$4SO_2 + 4H_2O = H_2S + 3H_2SO_4 \quad (3)$$

Previous work therefore suggests that SO_2 will react with water to produce dissolved sulfide, which will then reduce Fe^{III} to Fe^{II}, as the sulfide is oxidized to sulfate. In the absence of CO_2, additional sulfide will then react with dissolved Fe^{II} to produce solid Fe sulfide. The results presented herein assess whether dissolved CO_2, if available in sufficient quantities, competes more effectively than SO_2-derived dissolved sulfide for the dissolved Fe^{II}, resulting in precipitation of siderite rather than Fe sulfide (pyrite, FeS-am), and leaving the dissolved sulfide available for further reaction with and reduction of Fe^{III}.

Theoretical equilibrium calculations do not account for the kinetics of mineral dissolution and precipitation. Even if the products of a chemical reaction are favored thermodynamically, there is the possibility of precipitation and persistence of metastable phases. A common example is the precipitation of metastable amorphous silica rather than stable quartz during the cooling of silica-rich geothermal fluids. Herein, dissolution of CO_2 and SO_2 gases in water, and precipitation of siderite are all fast relative to rate limiting hematite dissolution. Because SO_2 dissolves quickly relative to hematite, the system is likely to be initially quite reducing, becoming more oxidizing as hematite continues to dissolve and react. A potential complication is that the initially highly reducing conditions may lead to precipitation of undesirable phases such as Fe sulfide or elemental S which are stable early in the reaction, but persist metastably later in the reaction and thereby prolong it. Ultimately, for the CO_2 trapping method described above to be viable, the absolute rate of siderite precipitation should, at a minimum, be sufficiently fast to be detected on the time scale of a laboratory experiment.

3. Methods

Two theoretical equilibrium geochemical simulations were constructed, identical except for the presence of a NaOH pH buffer. The simulations establish whether the siderite reaction product is favored thermodynamically, both with and without a pH buffer. A laboratory experiment was then carried out with the NaOH pH buffer. Sodium hydroxide was used in the experiment to simulate natural mineral buffering of pH, and to thereby increase the degree of siderite supersaturation and hence the siderite precipitation rates, so as to increase the probability of obtaining discernable siderite precipitation within several weeks. The computer simulation with the NaOH pH buffer provides a basis for comparison to establish the degree to which the experiment approaches equilibrium. The simulation without NaOH establishes whether the siderite reaction product is favored thermodynamically even in the absence of a pH buffer.

Modeled and experimental P–T conditions were 300 bar and 150 °C. Although the pressure is within the range typically found in sedimentary formations, the temperature is at the high end of the range that might be observed and was selected to increase reaction rates in the experiment. The initial aqueous phase was 150 ml (at 25 °C) of 1.0 m NaCl brine, with the NaOH concentration at 0.5 m in the pH-buffered simulation and the experiment. The initial solid phase was 10 g of hematite. The amount of initially anhydrous CO_2 was 16 g, a quantity sufficient to ensure the existence of excess supercritical CO_2 over the course of the reaction even if all of the Fe precipitated in siderite. The experiment used a fixed 2.5 g amount of SO_2, sufficient to reduce most but not all of the Fe. The simulations used incrementally increasing amounts of SO_2 (from 1.0 μg to 120 g) to show the effects of using SO_2 in quantities both less than, and far in excess of that required to reduce all of the Fe.

Hematite was used as the source of Fe^{III} in the experiment rather than natural Fe^{III}-bearing sediments, because the small volume of the experimental reaction cell severely limits the amount of Fe^{III} available if natural sediments were used. Use of a single, relatively pure hematite initial solid also facilitates detection of experimental reaction products. Therefore, hematite also also used in the simulations to facilitate comparison of the simulations to the experiment.

3.1. Modeling methods

The thermodynamic equilibrium simulations were computed using CHILLER (Reed, 1998), which calculates the distribution of chemical components among minerals, gases, and species in the aqueous phase. The sources of most of the thermodynamic data, the methods of computing activity and fugacity coefficients, and an overview of the limitations of the method are discussed in Palandri and Reed (2004) and are not repeated here. The thermodynamic data for minerals and H_2O and CO_2 gases are derived from the data of Holland and Powell (1998), and data for SO_2 and H_2S gases are derived from the SUPCRT92 data of Johnson et al. (1992). Data are not available to compute fugacity coefficients for SO_2 or H_2S and ideality is assumed. However, because SO_2 and H_2S are very soluble in aqueous fluids, the amount of these components in the gas phase is negligible and the gas phase is dominated by CO_2 and H_2O.

In the simulations the fluids were first equilibrated with hematite at the stated conditions, yielding a small amount of dissolved Fe^{III}. In the simulation without NaOH, equilibration with hematite yields a computed pH of 5.8, and upon further equilibration with excess supercritical CO_2, a pH of 3.3. In the simulation with NaOH, equilibration with hematite results in a pH of 10.9, and equilibration with excess CO_2 yields a pH of 5.9. The simulations were then completed by adding SO_2 incrementally and recalculating equilibrium at each step, to obtain the results discussed below. Although both gases should dissolve quickly, in the simulations all the CO_2 was added prior to incrementally adding SO_2, to assess the effects of varying amounts of SO_2 in CO_2-dominated flue gas.

3.2. Experimental methods

3.2.1. Experimental apparatus and set-up

The experiment was carried out in a flexible Au–Ti reaction cell with ~200 cm^3 total volume. The cell was contained within an autoclave which was secured within a cyclic rotating (180°) furnace. The assembly is equipped with a Ti-valved, Au-lined stainless steel capillary tube, that allows sampling of the fluid while maintaining experimental conditions in the reactor, and simultaneously allowing for rapid quenching of the sample. The brine volume was 150 ml at 25 °C (161 ml at 150 °C), and the brine was sparged for 2 h with N_2 to remove dissolved O_2. Hematite from Minas Gerais, Brazil was obtained from Ward's Natural Science Establishment, ground in an alumina disk mill, and sieved to obtain a 75–125 μm size fraction. X-ray diffraction (XRD) spectra confirmed the presence of hematite only. The fluid and 10 g of hematite were sealed inside the cell/autoclave/furnace assembly, and pressurized to 100 bar by adding water to the annulus surrounding the Au cell inside the autoclave. The CO_2 was injected with a syringe pump, the assemblage was heated to 150 °C, and the pressure was adjusted to 300 bar. Sulfur dioxide gas was then added with the syringe pump. Because of the high compressibility and the small volume of SO_2 used, there is considerable uncertainty in the amount added.

At the conclusion of the experiment at ~1400 h, 10 ml of 16.7 m NaOH was added to draw the remaining CO_2 into solution to avoid bursting the reaction cell. The autoclave was removed from the furnace and quenched with ~15 °C water until warm to the touch. The autoclave and reaction cell were disassembled, and the solids were filtered under vacuum through 2.5 μm paper filter then dried overnight at 80 °C. The NaOH addition, quench, reactor disassembly, and filtration were conducted in a period of less than 1 h.

3.3. Analytical methods

Aqueous samples were withdrawn from the experiment at various times for chemical analysis. Fluid pH was determined immediately; reported pH values are maxima because the fluid samples degassed CO_2 upon sampling. Dissolved sulfate and thiosulfate concentrations were determined by ion chromatography. Sulfite was detected but was not quantified because O_2 in the

chromatograph eluent leads to rapid sulfite oxidation. Total Fe and Fe^{II} concentrations were determined by the ferrozine colorimetric method after Stookey (1970), and Fe^{III} was calculated from the difference. $Iron^{II}$ values are minima because the samples were exposed to atmospheric O_2 for up to 30 min before analysis, possibly resulting in oxidation to Fe^{III}. Solids were analyzed by XRD to identify minerals, and by scanning electron microscopy with energy dispersive spectroscopy (SEM/EDS) to obtain backscatter images and semi-quantitative mineral chemical compositions. Solids for SEM/EDS analysis were mounted on 8–12 mm diameter sample holders by pressing the sample holders affixed with double-sided C impregnated tape into loose solid experimental products, and then coated with Au. Less than 5% of the solids were analyzed by SEM/EDS.

4. Results

4.1. Modeling results

In the first simulation (Fig. 1) without NaOH pH-buffering, siderite is stable over a wide range – almost 3 orders of magnitude – of total added SO_2 gas (Fig. 1(a)), from −2 to 0.95 log g (0.01–9 g). Pyrite replaces siderite, but only after hematite has dissolved completely. At equilibrium in this system, neither pyrite nor S can coexist with hematite. Although hematite and pyrite curves appear to overlap because of the finite line thickness, there is a short interval near 3.6 g (0.56 log g) SO_2 added where siderite is the only stable solid. Sulfur eventually replaces pyrite between 20 and 28 g (1.30 and 1.45 log g) SO_2 added. An important similar result is obtained in a simulation using H_2S instead of SO_2 (not shown in figures), but with higher pH and much lower sulfate concentration at any stage in the simulation.

Specific minerals can be suppressed from simulations where less stable phases are expected to precipitate because of their relative precipitation kinetics, e.g., suppression of quartz where amorphous silica is expected, and of pyrite and pyrrhotite where FeS-am is expected. Pyrite is not suppressed here to show that the most stable of the Fe sulfides (pyrite) is a less stable repository for Fe^{II} than siderite. If pyrite and pyrrhotite are suppressed (not shown) then S precipitates directly after siderite dissolution, and FeS-am does not precipitate. Although the dissolved Fe^{II} concentration is quite high, the dissolved sulfide concentration remains too low to reach FeS-am saturation.

The pH (Fig. 1(b)) increases from an initial value of 3.3, to 3.7, where siderite precipitates because hematite dissolution consumes H^+. Both siderite precipitation and SO_2 addition produce H^+ which leads to a steady decrease in pH to ~2.7. Where siderite begins to dissolve and consume H^+, the pH levels off slightly. The pH then begins to decrease more sharply once siderite dissolves out. A significant finding is that the total dissolved sulfide concentration, dominated by H_2S, remains less than 10 ppb until siderite dissolves completely, then increases to ~30–300 ppm, where pyrite is stable, and to ~600 ppm where native S is stable. The total dissolved Fe concentration increases steadily over the course of the simulation, exceeding 31,000 ppm where pyrite dissolves. Iron is present predominantly as Fe^{2+}, $FeCl^+$ and $FeSO_4$(aq). Total sulfate increases steadily over the course of the simulation, and is present mostly as SO_4^{2-}, $NaSO_4^-$, HSO_4^-, and $FeSO_4$(aq). The concentrations of thiosulfate and sulfite species are low, and just before hematite dissolves out, are both <0.01 ppm.

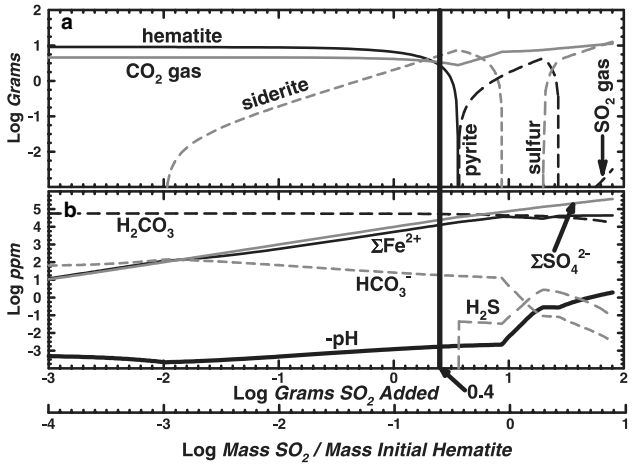

Fig. 1. Results summary from simulation at 150 °C and 300 bar of the CO_2–SO_2 reaction with 10 g of hematite in 156 g of 1.0 m NaCl brine using 14 g (excess) CO_2; vertical line at 0.4 log g (2.5 g) denotes the amount of SO_2 used in the experiment. (a) Mineral/gas phase assemblage. (b) Fluid composition.

In comparing the first and second (Fig. 2) simulations, without and with pH buffering respectively, the most significant difference is that with pH buffering, siderite is stable over a much wider range of SO_2 gas added (Fig. 2(a)) from 1 μg (off-scale left) to 16 g (−6.0 to 1.20 log g). Other differences with pH buffering include a much higher pH of ~6 (Fig. 2(b)) and much lower dissolved Fe^{II} concentration that results from increased siderite precipitation at higher pH. Total Fe remains constant near ~0.05 ppm where the simulation is pH buffered, increasing sharply to ~31,000 ppm where siderite dissolves out, then to ~34,000 ppm, where pyrite dissolves out. In the unbuffered simulation, the total Fe concentration increases steadily with increasing SO_2 added. The simulations are quite similar after ~0.4 log g SO_2 are added because the pH buffer in the second simulation has been overwhelmed by the addition of acidic SO_2. It can be concluded that at equilibrium, siderite is expected to reach saturation over a wide range of SO_2 gas added, and that this range is even greater in the presence of a natural or synthetic pH buffer.

The vertical line in Fig. 2 at 0.4 log g (2.5 g) added SO_2 denotes the system composition in the experiment if it reaches equilibrium, where the mineral assemblage should consist only of hematite and siderite. As in the first simulation above, there is a short interval near 0.603 log g SO_2 added where siderite is the only stable solid. Again, as for the first simulation, a similar result is obtained in a simulation using H_2S instead of SO_2 (not shown), but with higher pH and lower sulfate concentration.

4.2. Experimental results

Analyses of the experimental solids confirm that mixtures of CO_2 and SO_2 will reduce Fe^{III} in hematite to dissolved Fe^{II}, and precipitate Fe^{II} as siderite. Alteration minerals include siderite, pyrite, dawsonite ($NaAlCO_3(OH)_2$), and elemental S. XRD spectra verified only the presence of hematite and pyrite, and SEM/EDS verified the presence of the other reaction products. Very fine-grained (<500 nm) pyrite and/or FeS-am, and minor S also occur as a mixture of free grains (not shown in figures) not attached to hematite grains. EDS analysis of the mixture showed the presence of both Fe and S, and optical microscopy showed mostly gray-black mineral grains and a small number of yellow S grains. The identity of the Fe sulfide phase(s), however, could not be confirmed. In comparing the simulated and experimental alteration assemblages, the coexistence of pyrite and S with hematite in the experiment clearly indicates that the experiment is far from equilibrium after almost two months.

All of the hematite grains show some evidence of etching, but most do not show the presence of the alteration minerals on their surfaces, except for extremely fine-grained siderite and dawsonite that presumably precipitated rapidly after concentrated NaOH was added just prior to quenching the experiment. Some hematite grain surfaces show the presence of siderite, dawsonite and pyrite on the same grain (Fig. 3). Aluminum in dawsonite was likely derived from hematite, which can contain significant amounts of Al_2O_3 in solid solution, e.g., 10 wt% for hematite formed at 1000 °C (Deer et al., 1992). Alternatively, Al may have been provided by a contaminant phase(s) present in quantities insufficient to be detected by XRD spectra of the initial solids. It is unlikely that the alumina disk mill used for grinding the hematite provided Al in quantities sufficient to account for the amount of dawsonite observed.

A few of the hematite grains apparently were more efficient than others as nucleation sites, and are host to

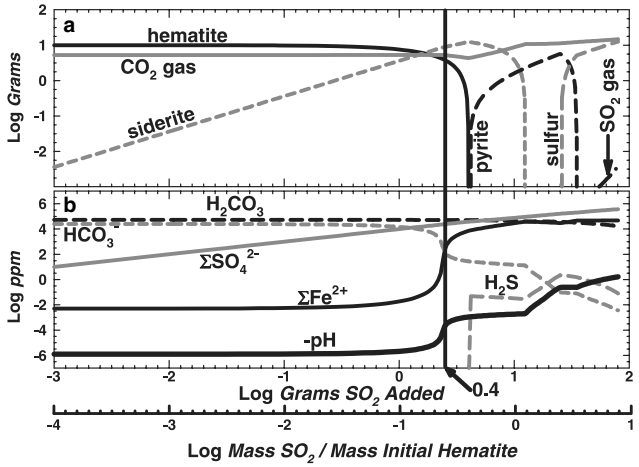

Fig. 2. Results summary from pH-buffered simulation at 150 °C and 300 bar of the CO_2–SO_2 reaction with 10 g of hematite in 159 g of 1.0 m NaCl, 0.5 m NaOH brine using 14 g (excess) CO_2; 0.4 log g (2.5 g) is the amount of SO_2 used in the experiment. (a) Mineral/gas phase assemblage. (b) Fluid composition.

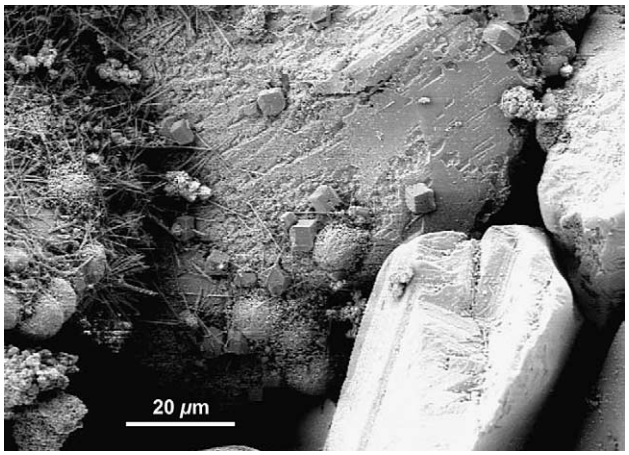

Fig. 3. Experimental results, solids: Rhombic (trigonal) siderite, acicular dawsonite, framboidal pyrite on etched hematite. Note clumps of fine-grained sulfur and siderite at lower left, upper right.

many crystals of siderite (Figs. 4 and 5). It is unclear why the siderite crystals in Fig. 4 show a stepped morphology while those in Fig. 5 do not. The presence of well-crystallized siderite as in Figs. 3 and 5 suggests that siderite precipitated slowly, rather than in the short period of time between the addition of NaOH and filtration of the solids at the end of the experiment.

Many of the hematite grains are host to framboid-like pyrite (Fig. 6). Also observed are either discrete hematite-free clumps composed of native S and minor siderite (Fig. 7), or, possibly, hematite grains where the number and size of siderite and S crystals are sufficient to completely obscure the hematite surface. The presence of siderite partially enclosed by S (Fig. 7) suggests that the S continued to grow after nucleation and growth of siderite, and provides further evidence that siderite nucleated and grew before concentrated NaOH was added prior to quenching the experiment. Sulfur appears to have been re-dissolving, because S crystals show rounding of edges ranging from moderate (Fig. 7) to pronounced (Fig. 8). Estimated mineral abundances by volume are ~90–95% unreacted hematite, 5–10% pyrite, 1–2% S, and 0.1–0.5% siderite.

The changes in fluid composition over the course of the experiment are summarized in Fig. 9. The Fe concentration (Fig. 9(a)) was initially high due to adhering surface fines after grinding the hematite. The total Fe concentration after 17 h was 320 ppm, which decreased rapidly to 12 ppm after 40 h. Total Fe then increased to 450 ppm at ~610 h, then decreased to 190 ppm at ~970 h, and remained approximately constant for the remainder of the experiment which was terminated at ~1400 h. Total dissolved Fe was dominated by Fe^{II} rather than Fe^{III} over most of the experiment. In the two instances where Fe

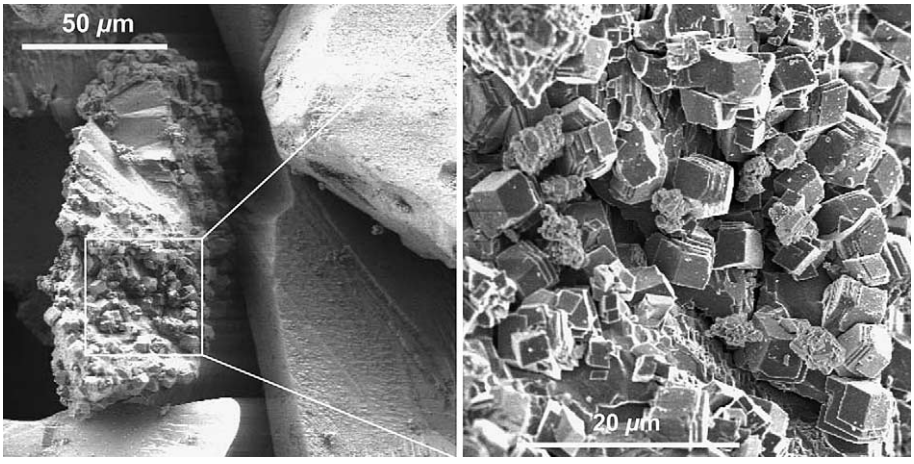

Fig. 4. Experimental results, solids: Siderite on etched hematite. Note stepped morphology to siderite crystals.

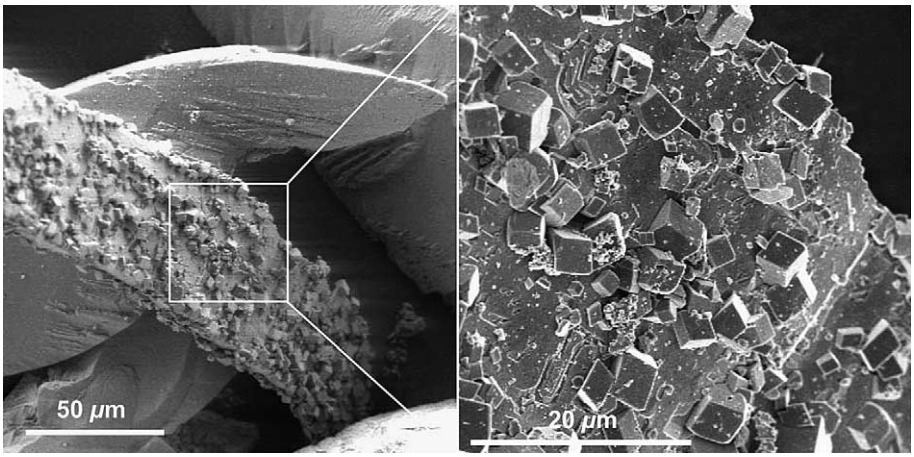

Fig. 5. Experimental results, solids: siderite on etched hematite. Note absence of stepped morphology to siderite crystals as in Fig. 4.

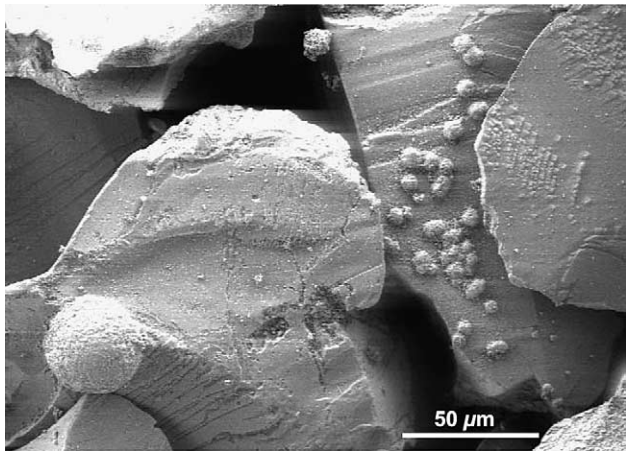

Fig. 6. Experimental results, solids: framboidal pyrite on etched hematite.

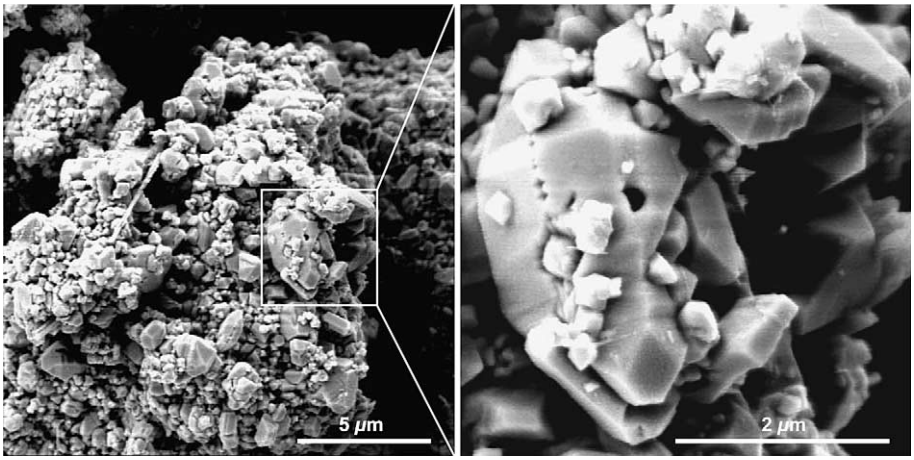

Fig. 7. Experimental results, solids: fine-grained clumps of dipyramidal sulfur with minor siderite. Note siderite crystal partly enclosed by sulfur, and rounding of sulfur grain suggesting dissolution.

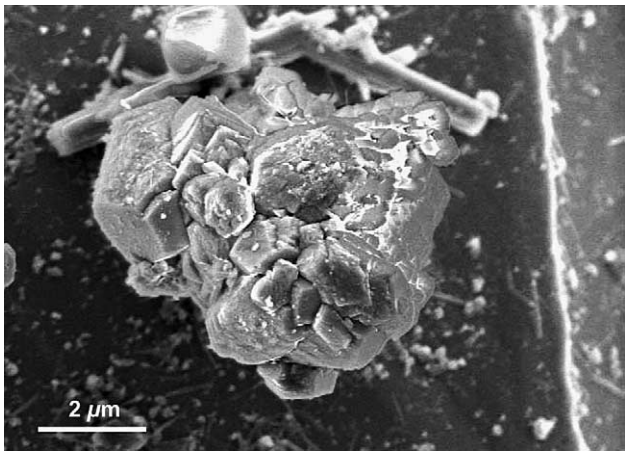

Fig. 8. Experimental results, solids: sulfur and tabular dawsonite on etched hematite. Note pronounced rounding of sulfur grain suggesting dissolution.

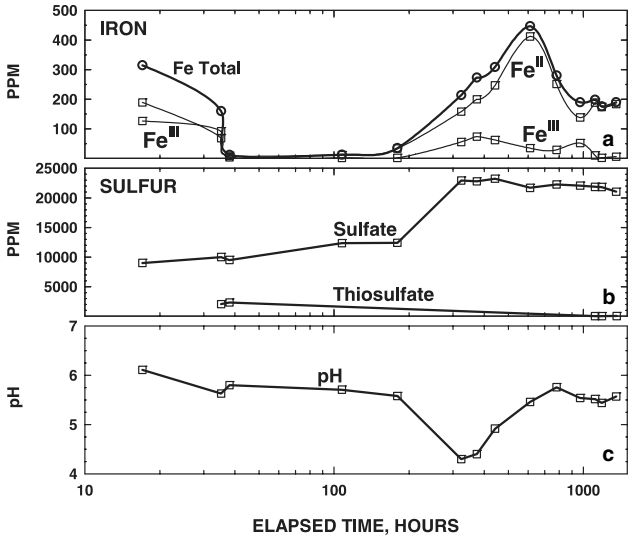

Fig. 9. Experimental results, fluid composition. (a) Dissolved iron: total iron, ferrous iron, ferric iron. (b) Dissolved sulfur: sulfate, thiosulfate. (c) Fluid pH, values are maxima due to CO_2 degassing upon sampling.

began to decrease at ~17 and ~610 h, it is apparent that dissolved Fe had increased to a point where nucleation of an Fe-bearing mineral has occurred and growth was proceeding. Given that nucleation and growth of amorphous Fe sulfide is fast at up to 71 °C (Palandri, 2000; Schoonen and Barnes, 1991) and that of siderite is relatively slow at up to 80 °C (Greenberg and Tomson, 1992; Jensen et al., 2002; Jimenez-Lopez and Romanek, 2004), it is likely that an Fe sulfide phase nucleated at ~17 h, and siderite at ~610 h.

Concentrations of dissolved S species are shown in Fig. 9(b). Disproportionation lead to high concentrations of sulfate and thiosulfate after 17 h. As mentioned above, sulfite was also detected but not quantified. However, the sulfite chromatograph peak areas appeared to decrease over the course of the experiment, indicating decreasing sulfite concentration. The odor of sulfide was not detected in any of the fluid samples over the course of the experiment, but a faint odor of sulfide was detected upon opening the reaction cell at the end of the experiment, indicating either the presence of a minute quantity of sulfide during the reaction, or that sulfide was produced by S or Fe sulfide dissolution during quenching. Disproportionation in the experiment apparently produces sulfate with thiosulfate and sulfite, as compared with sulfate, sulfide and only traces of thiosulfate and sulfite in the simulations. Sulfite reacts quickly with sulfide to produce thiosulfate (at 65 °C,

Schoonen and Barnes, 1991), so sulfide produced in the experiment may have reacted with excess sulfite producing thiosulfate and leaving a small amount of remaining sulfite. Sulfur not represented in Fig. 9(b) is likely contained in dissolved sulfite or elemental S.

The fluid pH (Fig. 9(c)) was measured as quickly as possible after fluid sampling. The pH values are maxima because the fluid degasses CO_2 upon sampling, leading to increased pH. However, decreased pH values near 4.3 centered around ~320 h likely resulted from S dissolution or possibly Fe sulfide dissolution. The pH then recovered to approximately its original value apparently due to continued hematite dissolution which consumed H^+.

5. Discussion

The equilibrium computer simulations indicate that for any amount of SO_2 added to this system, hematite cannot coexist with pyrite or S, and siderite cannot coexist with S. The coexistence of all 4 minerals in the laboratory experiment thus indicates a metastable system. There was a high degree of uncertainty in the amount of SO_2 added to the experiment, but, if the amount added was 2.5 g as intended, then hematite and siderite were stable, and pyrite and S were metastable. Pyrite was stable early in the experiment when little of the hematite had dissolved. Dissolution features were not observed on pyrite grains, so depending on the amount of SO_2 added, pyrite could have been stable at the end of the experiment, or re-dissolving too slowly to be develop dissolution features. FeS-am if present, is always metastable with respect to pyrite and should re-dissolve. Elemental S could also have been stable early in the experiment, or could have been produced as a metastable intermediate of the SO_2 reaction with water. Sulfur in the experiment was apparently re-dissolving, and given enough time it would likely dissolve completely. Further dissolution of S and possibly pyrite should lead to further reduction of Fe^{III} from hematite and hence further precipitation of siderite. In any case, hematite was unstable and continued to dissolve over the course of the experiment, while siderite apparently became stable enough at ~610 h to nucleate, then continued to grow until the end of the experiment. If Fe^{III}-bearing phases such as FeO·OH that dissolve more quickly than hematite were present, as might occur with thin grain coatings with large surface area as in redbeds, the overall reaction may proceed more quickly than observed for hematite.

The desired molar ratio for CO_2 to SO_2 indicated by Eq. (1) is 2:1, but the ratio in the simulation where all of the hematite has been consumed is near 3:1 (excluding the CO_2 remaining in the supercritical gas phase) because a large amount of CO_2 remained dissolved in solution. Therefore a significant limitation in using Fe^{III} to sequester CO_2 from power plants is that flue gas derived from the combustion of fossil fuel, even coal with high S content, typically contains less than 5.0 wt% SO_2, and would not contain enough SO_2 to reduce Fe in quantity sufficient to trap all of the CO_2 in siderite if sufficient Fe^{III} is present. To trap all of the CO_2 in such a gas in carbonate minerals, targeted sediments must contain other divalent metals capable of precipitating out CO_2, but not already bound in carbonate minerals, e.g., Ca, Mg, or already reduced Fe^{II}. Decreased pH due to acid gas addition may increase the solubility of carbonate minerals containing these cations thereby preventing their precipitation, but in that case C would be stored in the fluid as dissolved HCO_3^-. Alternatively, reduced S-bearing waste gas derived from other industrial processes, e.g., H_2S from sour natural gas processing, could be added to the waste gas stream. Given that production of hydrocarbon syn-fuels from coal gasification also produces CO_2 and H_2S waste, this waste could be disposed of in a similar manner. If Fe is absent from the targeted rocks, SO_2, but not H_2S, will apparently be converted to less toxic and less reactive elemental S, and might still be disposed of without first separating SO_2 from CO_2.

Mineral dissolution and precipitation may affect the hydrologic properties of targeted aquifers. Considering only volume changes, mineral dissolution and precipitation result in porosity (and permeability) and increase and decrease, respectively. Hematite and siderite have molar volumes of 30.3 and 29.4 cm^3, respectively (Holland and Powell, 1998), and, therefore, complete alteration of hematite to siderite would lead to almost a doubling of mineral volume. A redbed composed dominantly of quartz with 1% hematite and having 20% porosity would show less than 1% porosity decrease. However, dissolution of mineral cements may lead to release of detritus that would clog pore throats and lead to a permeability decrease. There may also be a porosity and permeability loss near the site of injection due to S precipitation. Further, because of the high concentration of dissolved sulfate, the presence of Ca in sediments may lead to the precipitation of anhydrite or gypsum, which could also lead to a decrease in porosity and permeability. The presence of Ca may also lead to the precipitation of ankerite instead of siderite. No statement can be made regarding volume changes in rocks where reactant Fe^{III} is contained in other minerals without knowledge of the mineral identity and composition.

6. Summary and conclusions

Theoretical equilibrium calculations predict that 2 mol of CO_2 and 1 mol of SO_2 gases will react with Fe^{III} in 1 mol of hematite, to produce the Fe^{II} in 2 mol of siderite, effectively trapping the CO_2. Accounting for CO_2 remaining in solution yields a higher ratio of CO_2 to

SO_2, depending on the water–rock ratio. If there is less SO_2, not all of the hematite will dissolve, and not all of the CO_2 will be trapped. If there is more SO_2, more or all of the Fe will reside in solution and/or solid Fe sulfide, and again not all of the CO_2 will be trapped. At the appropriate CO_2:SO_2, S will reside only in dissolved sulfate. The presence of an alkaline pH buffer enhances the stability of siderite so that it is stable over a greater range of SO_2 gas added.

The predictions based on computer simulations are largely confirmed by experimental results, and siderite eventually became stable under the conditions specified. However, the experiment did not reach equilibrium after two months at 150 °C and 300 bar, as indicated by the presence of two early formed metastable phases, pyrite and elemental S. In the experimental fluid, metastable thiosulfate and sulfite which decreased with time, were also detected in addition to stable sulfate. Experimental results are consistent with nucleation of metastable pyrite near 17 h, nucleation of metastable S before 611 h, and nucleation of siderite near 611 h. Precipitated S apparently re-dissolves, and pyrite should re-dissolve as well, allowing for further Fe reduction and siderite precipitation. Given sufficient time on the order of years to tens of years, the reaction should reach equilibrium. The authors suggest that Fe^{III} in minerals other than hematite in sedimentary rocks will also serve as CO_2 mineral traps, if reduced S-bearing gas such SO_2 or H_2S is introduced with the CO_2.

Acknowledgments

We thank Andy Ouimette for assistance in preparation of the experimental solids, and Gil Ambats, Monami Datta, Mark Huebner, and Evangelos Kakouros for their assistance in sampling and analysis of the experimental fluids. We also thank Robert Oscarson for his assistance with the SEM/EDS in analysis of the experimental solids. Thanks are also due to William Evans, Robert Mariner, Mark Reed, Applied Geochemistry associate editor Ian Hutcheon, and two anonymous reviewers for suggestions and comments which have led to substantial improvement of this manuscript. This work is supported in part by the US Department of Energy (DOE Grant DE-AI26-01NT4116).

References

Bergman, P.D., Winter, E.M., 1995. Disposal of carbon dioxide in aquifers in the US. Energy Convers. Manage. 36, 523–526.

Bruant Jr., R.G., Guswa, A.J., Celia, M.A., Peters, C.A., 2002. Safe storage of CO_2 in deep saline aquifers. Environ. Sci. Technol. 36, 240A–245A.

Deer, W.A., Howie, R.A., Zussman, J., 1992. An Introduction to the Rock-Forming Minerals. Longman, Essex.

Falkowski, P., Scholes, R.J., Boyle, E., Canadell, J., Canfield, D., Elser, J., Gruber, N., Hibbard, K., Hogberg, P., Linder, S., Mackenzie, F.T., Moore, B.I., Pedersen, T., Rosenthal, Y., Seitzinger, S., Smetacek, V., Steffen, W., 2000. The global carbon cycle: a test of our knowledge of Earth as a system. Science 290, 291–296.

Getahun, A., Reed, M.H., Symonds, R., 1996. Mount St. Augustine Volcano fumarole wall rock alteration: mineralogy, zoning, composition and numerical models of its formation process. J. Volcanol. Geotherm. Res. 71, 73–107.

Greenberg, J., Tomson, M., 1992. Precipitation and dissolution kinetics and equilibria of aqueous ferrous carbonate vs temperature. Appl. Geochem. 7, 185–190.

Gunter, W.D., Wiwchar, B., Perkins, E.H., 1997. Aquifer disposal of CO_2-rich greenhouse gases: extension of the time scale of experiment for CO_2-sequestering reactions by geochemical modeling. Mineral. Petrol. 59, 121–140.

Gunter, W.D., Perkins, E.H., Hutcheon, I., 2000. Aquifer disposal of acid gases: modelling of water–rock reactions for trapping of acid wastes. Appl. Geochem. 15, 1085–1095.

Harrison, W.J., Wendlandt, R.F., 1995. Geochemical interactions resulting from carbon dioxide disposal on the seafloor. Appl. Geochem. 10, 461–475.

Hitchon, B., 1996. Aquifer Disposal of Carbon Dioxide. Hydrodynamic and Mineral Trapping-proof of Concept. Geoscience Publishing Ltd., London.

Holland, T.J.B., Powell, R., 1998. An internally consistent thermodynamic data set for phases of petrological interest. J. Metamorph. Geol. 16, 309–343.

Jensen, D.L., Boddum, J.K., Tjell, J.C., Christensen, T.H., 2002. The solubility of rhodochrosite ($MnCO_3$) and siderite ($FeCO_3$) in anaerobic aquatic environments. Appl. Geochem. 17, 503–511.

Jimenez-Lopez, C., Romanek, C.S., 2004. Precipitation kinetics and carbon isotope partitioning of inorganic siderite at 25 °C and 1 atm. Geochim. Cosmochim. Acta 68, 557–571.

Johnson, J.W., Oelkers, E.H., Helgeson, H.C., 1992. SUPCRT92: A software package for calculating the standard molal thermodynamic properties of minerals, gases, aqueous species, and reactions from 1 to 5000 bar and 0 to 1000 °C. Comput. Geosci. 7, 899–947.

Johnson, J.W., Nitao, J.J., Steefel, C.I., Knauss, K.G., 2001. Reactive transport modeling of geologic CO_2 sequestration in saline aquifers: the influence of intra-aquifer shales and the relative effectiveness of structural, solubility, and mineral trapping during prograde and retrograde sequestration. In: Proceedings, First National Conference on Carbon Sequestration. May 14–17, 2001, Washington, DC.

Kaszuba, J.P., Janecky, D.R., Snow, M.G., 2003. Carbon dioxide reaction processes in a model brine aquifer at 200 °C and 200 bars: implications for geologic sequestration of carbon. Appl. Geochem. 18, 1065–1080.

McPherson, B.J.O.L., Cole, B.S., 2000. Multiphase CO_2 flow, transport and sequestration in the Powder River Basin, Wyoming, USA. J. Geochem. Explor. 69–70, 65–69.

Palandri, J.L., 2000. Applications of computed chemical equilibria: I. Reconstruction of in situ composition of sedimentary formation waters; II. Disposal of H_2S from natural gas; III. Serpentinization, related rodingitization,

and silica-carbonate alteration of ultramafic rock. Ph.D thesis, University of Oregon.

Palandri, J.L., Reed, M.H., 2004. Geochemical models of metasomatism in ultramafic systems: serpentinization, rodingitization, and sea floor carbonate chimney precipitation. Geochim. Cosmochim. Acta 68, 1115–1133.

Pruess, K., Xu, T., Apps, J., Garcia, J., 2001. Numerical modeling of aquifer disposal of CO_2. In: Proceedings, SPE/EPS/DOE Exploration and Environmental Conference, San Antonio, TX, pp. 1–14.

Reed, M.H., 1998. Calculation of simultaneous chemical equilibria in aqueous-mineral-gas systems and its application to modeling hydrothermal processes. In: Richards, J., Larson, P. (Eds.), Techniques in Hydrothermal Ore Deposits Geology. Economic Geology, Socorro, NM, pp. 109–124.

Schoonen, M.A.A., Barnes, H.L., 1991. Reactions forming pyrite and marcasite from solution: II. Via FeS precursors below 100 °C. Geochim. Cosmochim. Acta 55, 1505–1514.

Spycher, N., Pruess, K., Ennis-King, J., 2003. CO_2–H_2O mixtures in the geological sequestration of CO_2. I. Assessment and calculation of mutual solubilities from 12 to 100 °C and up to 600 bar. Geochim. Cosmochim. Acta 67, 3015–3031.

Stookey, L.L., 1970. Ferrozine – a new spectrophotometric reagent for iron. Anal. Chem. 42, 779–782.

Symonds, R., Gerlach, T., Reed, M., 2001. Magmatic gas scrubbing: Implications for volcano monitoring. J. Volcanol. Geotherm. Res. 108, 303–341.

White, C.M., Strazisar, B.R., Granite, E.J., Hoffman, J.S., Pennline, H.W., 2003. Critical review: separation and capture of CO_2 from large stationary sources and sequestration in geological formations – coalbeds and deep saline aquifers. J. Air Waste Manage. 53, 645–715.

Wolf, G.H., Chizmeshya, A.V.G., Diefenbacher, J., McKelvy, M.J., 2004. In situ observation of CO_2 sequestration reactions using a novel microreaction system. Environ. Sci. Technol. 38, 932–936.